Feasiblity of Motion Primitives for Choreographed Quadrocopter Flight

Angela Schöllig, Markus Hehn, Sergei Lupashin and Raffaello D'Andrea

Abstract— This paper describes a method for checking the feasibility of quadrocopter motions. The approach, meant as a validation tool for preprogrammed quadrocopter performances, is based on first principles models and ensures that a desired trajectory respects both vehicle dynamics and motor thrust limits. We apply this method towards the eventual goal of using parameterized motion primitives for expressive quadrocopter choreographies. First, we show how a large class of motion primitives can be formulated as truncated Fourier series. We then show how the feasibility check can be applied to such motions by deriving explicit parameter constraints for two particular parameterized primitives. The predicted feasibility constraints are compared against experimental results from quadrocopters in the ETH Flying Machine Arena.

I. INTRODUCTION

Our goal is to derive motion primitives for quadrocopter flight choreography, where we define 'choreography' as the design and arrangement of expressive sequences of movements.

Motion primitives are short and fairly simple basic motion elements; when concatenated, they can describe complex behavior and are often used to represent repetitive movements such as, for example, human hand-writing [1] or human body gestures [2]. Motion primitives are also used as a tool for simplifying complex problems, including motion planning [3]–[5], the control of humanoid robots [6]–[8], object recognition in video [9] or motion extraction from large data sets [10]. In particular, dance movement is often described by motion primitives because of its repetitive and rhythmic form [11]–[14].

In this paper, we introduce motion primitives as basis elements for choreographed dance-like quadrocopter movements. The design of these primitives is guided by the four key variables of dance as described by professional dancers and choreographers: time, space, energy, and structure. We present motion primitives that are adjustable in their temporal characteristics as well as in their spatial features. A wide spectrum of movements and motion segments are included in the library of motion primitives, ranging from sharp and energetic movements to soft and smooth ones. With this library, we aim at providing a choreographer with degrees of freedom for creating an expressive choreography comparable to a human dance performance.

Like humans, whose range of motion and speed of movement is limited, not all motions are feasible for a quadrocopter. Thus, a large part of the analysis below is devoted to determining the set of parameters that represents

The authors are with the Institute for Dynamic Systems and Control, ETH Zurich, 8092 Zurich, Switzerland. (aschoellig,hehnm,sergeil,rdandrea)@ethz.ch
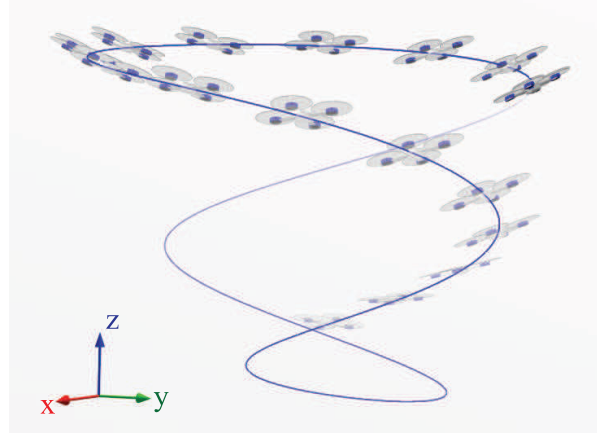
Fig. 1. An example of a periodic motion primitive studied in this paper.

motion sequences that can be realized with a quadrocopter. The resulting library of feasible motion primitives allows for multifaceted choreographies that could eventually be synchronized to music, in order to create a novel visual musical experience as described in [15].

This paper is organized as follows: Sec. II introduces a general description for motion primitives that define the translational dynamics of the quadrocopter and can be related to the four key elements of dance. In Sec. III, the equations governing the dynamic behavior and constraints of the quadrocopter are stated. This allows us to derive inequalities for determining the feasibility of trajectories in Sec. IV. To illustrate the effectiveness of this procedure, feasible parameter sets are explicitly calculated for two motion primitives and validated by experimental data (Sec. V). We conclude the paper with a summary in Sec. VII.

II. MOTION PRIMITIVES

Our goal is to develop basic motion elements that – when combined into sequences – allow for a multifaceted, meaningful quadrocopter choreography. We specify motion primitives on the quadrocopter's translational position $s(t) = (x(t), y(t), z(t))$ measured in the inertial coordinate system $\mathbf{O}$, see Fig. 2. The remaining degrees of freedom, namely the vehicle's attitude $\mathbf{V}$, are not considered in the description of the motion primitive, but are partly defined by the quadrocopter's dynamics, see Sec. III. Motion primitives are introduced as

$$s_d(t) = s_d(p, t), \tag{1}$$

over a finite time interval $t \in [t_0, t_f] \subset \mathbb{R}$, $t_f < \infty$, where p denotes the set of adjustable motion parameters. Parameterized motion primitives allow for variety and expressiveness

in the choreography design and provide choreographers with intuitive tools for the design of performances.

Our objective is to offer a similar range of motions as is used in human dance composition. In this context, we ask: Which choices does a professional dance choreographer have when creating a performance? How can we provide the tools and degrees of freedom necessary for implementing an expressive performance on the quadrocopter?

Four fundamental choreographic elements – time, space, energy, and structure – are commonly used by professional dancers, choreographers and dance teachers to build choreography with interest, dynamics and aesthetic appeal, cf. [16], [17]. These parameters provide a framework for meaningful quadrocopter choreography, and are described as follows:

Space – Space refers to the area the dancer is performing in. It also relates to how the dancer moves through the area, as characterized by the direction and path of a movement, as well as its size, level, and shape.

Time – Time encompasses rhythm, tempo, duration, and phrasing of movements. Using time in different combinations can create intricate visual effects. Ideas such as quick-quick, slow or stop movements are examples.

Energy – Energy relates to the quality of movement. This concept is recognizable when comparing ballet and tap dance. Some types of choreography are soft and smooth, while others are sharp and energetic.

Structure – Structure represents the organization of movement sequences into larger concepts: the combination and variation of movements using recurring elements, contrast, and repetition. Movements can even follow a specific story line to convey certain information through a dance.

Examples illustrating the four elements of dance are found in [16], [17].

One way of introducing parameterized motion primitives that capture a wide range of different movements is as a Fourier series [18],

$$s_d(t) = a_0 + \sum_{k=1}^{N} a_k \cos\left(k\,\Omega t\right) + b_k \sin\left(k\,\Omega t\right), \quad (2)$$

where $\Omega = 2\pi/T$ represents the fundamental angular frequency corresponding to a period of T. Additional design parameters are the constant vectors $a_0, a_k, b_k \in \mathbb{R}^3$, $k \in \mathcal{K} = \{1, 2, \dots, N\}$, and $N \geq 1$; that is, $p = \{\Omega, N, a_0, a_k, b_k \mid k \in \mathcal{K}\}$. The parameters p allow us to express the key choreographic elements:

Space – The parameters a_0 and a_k, b_k, $k \in \mathcal{K}$ define the amplitudes of the periodic motion and, thus, the spacial dimension of the movement. These vectors also specify the direction of the motion and the overall three-dimensional shape of the curve.

Time – The underlying rhythm is given by the frequency Ω. When the choreography is set to music, the frequency Ω can be related to the music's tempo. Different tempos are combined when choosing $N > 1$. The overall duration of the motion can be adjusted via t_f.

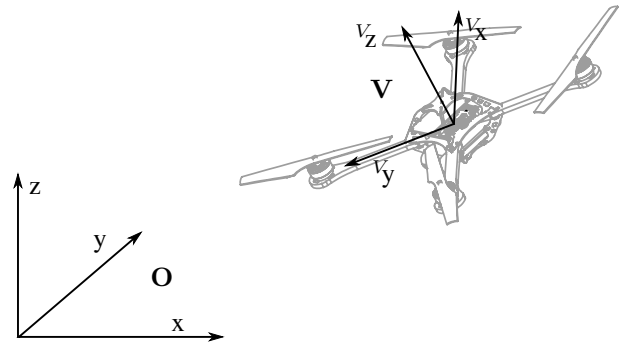**Energy** – The higher the value of N, the more energetic

Fig. 2. The inertial coordinate system **O** and the vehicle coordinate system **V**.

and sharp are the possible motions, cf. [18].

Structure – The motion primitives described in (2) can be combined into sequences, which can in turn be combined to create an overall choreographic performance. Endless permutations are possible, much the way individual words can be combined into a variety of sophisticated stories.

In short, the general motion description (2) reflects the fundamental choregraphic elements and allows for a multi-dimensional choreography. Out of the variety of motions captured by (2), Fig. 1 illustrates the one with $N = 3$, $T = 10$, $a_0 = (0, 0, 3)$, $a_1 = (0, 0, 1)$, $a_2 = (1, 0, 0)$, $b_3 = (0, 1, 0)$ and a_3, b_1, b_2 being zero. A Matlab file for generating arbitrary motion primitives of the proposed type are available online at www.idsc.ethz.ch/Downloads/QuadDance.

In order to make (1) and (2) a useful tool for choreographers, we need to specify which motion primitives can be realized on the vehicle. The dynamics and physical limits of the quadrocopter define the feasible sets of parameters p.

III. QUADROCOPTER DYNAMICS AND CONSTRAINTS

The quadrocopter dynamics and constraints are derived from first principles models:

A. Dynamics

The quadrocopter is described by six degrees of freedom: The translational position $s = (x, y, z)$ is measured in the inertial coordinate system **O** as shown in Fig. 2. The vehicle attitude is defined by the body-fixed frame **V** and represented by the Euler angles yaw, pitch and roll, (α, β, γ). The rotation matrix $_V^O R(\alpha, \beta, \gamma)$ for transforming coordinates from **V** to **O** is

$$_V^O R(\alpha, \beta, \gamma) = R_z\left(\alpha\right) R_y\left(\beta\right) R_x\left(\gamma\right), \quad (3)$$

where

$$R_x\left(\gamma\right) = \begin{bmatrix} 1 & 0 & 0 \\ 0 & \cos\gamma & -\sin\gamma \\ 0 & \sin\gamma & \cos\gamma \end{bmatrix}, \quad (4)$$

$$R_y\left(\beta\right) = \begin{bmatrix} \cos\beta & 0 & \sin\beta \\ 0 & 1 & 0 \\ -\sin\beta & 0 & \cos\beta \end{bmatrix}, \quad (5)$$

$$R_z(\alpha) = \begin{bmatrix} \cos\alpha & -\sin\alpha & 0 \\ \sin\alpha & \cos\alpha & 0 \\ 0 & 0 & 1 \end{bmatrix}. \qquad (6)$$

The vector s describes the center of mass of the vehicle in the inertial coordinate system $\mathbf{O}$. The translational acceleration of the vehicle is dictated by the attitude of the vehicle and the total thrust produced by the four propellers. The translational dynamics in the inertial frame are given by

$$\ddot{s} = {}^O_V R(\alpha, \beta, \gamma) \begin{bmatrix} 0 \\ 0 \\ f \end{bmatrix} - \begin{bmatrix} 0 \\ 0 \\ g \end{bmatrix}, \qquad (7)$$

where g is the acceleration due to gravity and f is the sum of the rotor forces F_i normalized by the vehicle mass m,

$$f = \sum_{i=1}^{4} f_i \qquad \text{with } f_i = F_i/m. \qquad (8)$$

The control inputs to the vehicle are the mass-normalized collective thrust f and the desired rotational rates about the vehicle body axes, $\omega = (\omega_x, \omega_y, \omega_z)$, see Fig. 3.

The relationship between the body-fixed angular velocity vector ω and the rate of change of the Euler angles is

$$\omega = \begin{bmatrix} \cos\beta\cos\gamma & -\sin\gamma & 0 \\ \cos\beta\sin\gamma & \cos\gamma & 0 \\ -\sin\beta & 0 & 1 \end{bmatrix} \begin{bmatrix} \dot{\gamma} \\ \dot{\beta} \\ \dot{\alpha} \end{bmatrix}. \qquad (9)$$

Each rotor of the quadrocopter produces not only a force F_i, $i \in \mathcal{I} = \{1, 2, 3, 4\}$, in the positive ${}^Vz$ direction, but also a reaction torque M_i perpendicular to the plane of rotation of the blade, see Fig. 3, where

$$M_i = kF_i, \qquad k = \text{const}, \qquad (10)$$

describes the relationship between the motor force F_i and the associated reaction torque M_i. The parameter k is given by the motor characteristics, see [19] for details. Rotors 1 and 3 rotate in the negative ${}^Vz$ direction, producing a moment that acts in the positive ${}^Vz$ direction; while rotors 2 and 4 rotate in the opposite direction resulting in reaction torques in the negative ${}^Vz$ direction. Given the inertia matrix I with respect to the center of mass and the vehicle frame $\mathbf{V}$, the rotational dynamics of the body-fixed frame are given by

$$I\dot{\omega} = \begin{bmatrix} L(F_2 - F_4) \\ L(F_3 - F_1) \\ k(F_1 - F_2 + F_3 - F_4) \end{bmatrix} - \omega \times I\omega, \qquad (11)$$

where L is the distance from each motor to the center of the quadrocopter. The vehicle's principal axes coincide with the vehicle frame axes, resulting in a diagonal inertia matrix with entries (I_x, I_y, I_z), where $I_x = I_y$ because of symmetry.

B. Constraints

The agility of the quadrocopter is constrained by the minimum and maximum force of a single motor,

$$f_{i,min} \le f_i \le f_{i,max}, \quad i \in \{1, 2, 3, 4\}, \qquad (12)$$

where we use the mass-normalized representation of the forces. The forces are always positive, $f_{i,min} \ge 0$, since the motors can spin only in one direction. Assuming identical
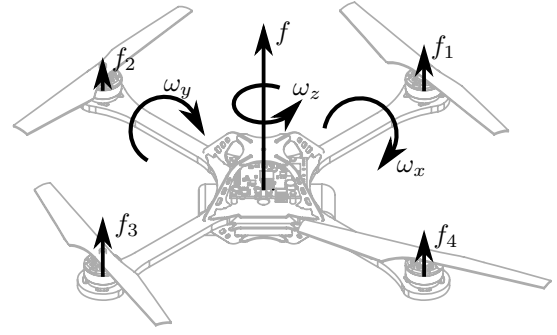

Fig. 3. The control inputs of the quadrocopter are the body rates ω_x, ω_y, and ω_z and the collective thrust f. These inputs are converted by an onboard controller into motor forces f_i, $i \in \{1, 2, 3, 4\}$.

motors, the collective thrust is bounded by

$$f_{min} \le f \le f_{max} \qquad (13)$$

with $f_{min} = 4f_{i,min}$ and $f_{max} = 4f_{i,max}$.

In the following feasibility analysis, we study the nominal dynamics of the vehicle under the assumption that we can control the vehicle body rates directly, and ignore rotational acceleration dynamics. We also assume that the collective thrust can be changed instantaneously.

We justify the above assumption based on experimental results that show a fast response time to changes in the desired rotational rates (time constants are on the order of 20 ms). A high-bandwidth controller on the vehicle tracks the desired rates using feedback from gyroscopes. Because the quadrocopter has very low rotational inertia and can produce high torques due to the outwards mounting of the propellers, see Tab. I, high rotational accelerations in the order of 200 rad/s² are achievable. The true thrust dynamics are as fast as the rotational dynamics, with propeller spin-up being faster than spin-down.

This allows us to calculate the motor forces $f_i(t)$ for a desired motion primitive from the nominal inputs, $\omega_d(t)$ and $f_d(t)$, using equations (8) and (11).

IV. FEASIBILITY OF MOTION PRIMITIVES

For the subsequent feasibility analysis, we assume that motion primitives, cf. (1), are twice-differentiable in time. Feasibility is formulated in terms of the motor limits $c = \{f_{i,min}, f_{i,max}\}$ and the motion parameters p. The objective is to derive a set of inequalities that specify feasible parameter sets p given the limits c,

$$\bar{h}(p, c, t) \le 0 \qquad \forall t \in [t_0, t_f]. \qquad (14)$$

In other words, given the vehicle limits c, a parameter set p is feasible if (14) is satisfied over the whole time interval $t \in [t_0, t_f]$.

The vehicle is constrained by the minimum and maximum force of a single rotor, cf. (12), which in turn results in a minimum and maximum collective thrust (13). Each of the aforementioned constraints must be satisfied in order to

guarantee the feasibility of a given motion primitive,

$$\bar{h}(p,c,t) = \begin{bmatrix} h(p,c,t) \\ h_1(p,c,t) \\ h_2(p,c,t) \\ h_3(p,c,t) \\ h_4(p,c,t) \end{bmatrix} \leq 0, \qquad \forall\, t \in [t_0, t_f]\,, \quad (15)$$

where $h(p,c,t)$ represents the constraint on the collective thrust (13) and $h_i(p,c,t)$, $i \in \mathcal{I}$ the motor limits (12). The above inequality is defined componentwise. Note that the inequalities on the single motors $h_i(p,c,t)$, $i \in \mathcal{I}$, alone would be sufficient for investigating the feasibility of a motion primitive. However, we keep $h(p,c,t)$, since this inequality can be can be derived directly from (7) and checked easily, as shown below.

A. Collective Thrust Limit

To derive $h(p,c,t)$ for a desired motion primitive s_d, we re-write (7),

$$_V^O R(\alpha,\beta,\gamma)\, n\, f_d = \ddot{s}_d + n\, g\,, \qquad (16)$$

where $n = \begin{bmatrix} 0,0,1 \end{bmatrix}$ and f_d is the nominal thrust input associated with s_d. Taking the 2-norm, we can solve for f_d, $f_d \geq 0$,

$$\left\| _V^O R(\alpha,\beta,\gamma)\, n\, f_d \right\| = \left\| \ddot{s}_d + n\, g \right\| \;\Leftrightarrow\; f_d = \left\| \ddot{s}_d + n\, g \right\|\,. \qquad (17)$$

Recalling that $s_d = s_d(p,t)$ and (13), the constraint guaranteeing the maximum and minimum bound of the collective thrust, is

$$h(p,c,t) = \begin{bmatrix} \left\| \ddot{s}_d(p,t) + n\, g \right\| - f_{max} \\ f_{min} - \left\| \ddot{s}_d(p,t) + n\, g \right\| \end{bmatrix} \leq 0\,. \qquad (18)$$

This feasibility requirement can be checked for any given desired motion primitive $s_d(p,t)$ by calculating its second time derivative. No further calculations are necessary. In particular, the nominal input associated with $s_d(p,t)$ need not be determined in advance. The constraint (18) on the collective thrust guarantees that the translational dynamics (7) are satisfied. Most importantly, it excludes the majority of infeasible parameters p. For a more detailed discussion on this topic see Sec. IV-C and the examples in Sec. V.

B. Motor Saturation

In order to evaluate the motor constraints (12), we must determine the (nominal) rotational inputs $\omega_d(t)$ of the given motion primitive $s_d(t)$. Given $\omega_d(t)$, we can, for the motor forces $f_{i,d}(t)$, $i \in \mathcal{I}$, solve a linear system of equations, (8) and (11), and check their feasibility based on (12). Note that in specifying a trajectory by its translational degrees of freedom, we are free to choose the rotational rate $\omega_z(t)$. For the general case (1), the rotational inputs $\omega_{x,d}(t)$ and $\omega_{y,d}(t)$ are obtained by numerically integrating the dynamic equations (7), (9) and (11), and using the result (17). Below, we propose problem-specific analytic solutions for two simple examples and state $h_i(p,c,t)$ explicitly.

C. Discussion

The collective thrust constraint $h(c,p,t)$ and the motor constraints $h_i(c,p,t)$ differ in the computational effort necessary for evaluating the corresponding inequalities as well as in the information they provide. The collective constraint $h(c,p,t)$ can be explicitly stated, see (18), is easy to evaluate, and provides quick insight into the dynamic behavior of the quadrocopter by excluding the majority of infeasible parameter sets. In contrast, for the motor constraints, we first need to calculate the nominal inputs $\omega_{x,d}(t)$ and $\omega_{y,d}(t)$. An explicit equation for $\omega_{x,d}(t)$ and $\omega_{y,d}(t)$ can be derived only in simple cases; in the general case, the rotational inputs are found numerically. The effects of both types of constraints are evident in the following two examples.

V. EXAMPLES

We consider two simple periodic motions that fall into the framework introduced in (2): a side-to-side motion and a circular motion in the horizontal plane. For the side-to-side motion, experimental results are shown in Sec. VI.

A. Side-to-Side Motion

The desired motion is a planar side-to-side movement,

$$s_d(t) = \begin{bmatrix} x_d(t) \\ y_d(t) \\ z_d(t) \end{bmatrix} = \begin{bmatrix} A\cos(\Omega t) \\ 0 \\ 0 \end{bmatrix}\,. \qquad (19)$$

The objective is to determine feasible combinations of amplitudes A and frequencies Ω. The side-to-side motion is a special case of the general motion primitive description (2), where $N = 1$, $a_1 = (A,0,0)$ and $a_0, b_1 = (0,0,0)$.

Calculating the second derivative of (19) and inserting it into (18), gives us the inequalities resulting from the collective thrust limit,

$$h(p,c,t) = \begin{bmatrix} \sqrt{A^2\Omega^4\cos^2\Omega t + g^2} - f_{max} \\ f_{min} - \sqrt{A^2\Omega^4\cos^2\Omega t + g^2} \end{bmatrix} \leq 0\,. \quad (20)$$

Given a pair (A,Ω), these inequalities must be satisfied for all $t \in [0,T]$. Therefore, it is enough to consider

$$\max_{t\in[0,T]} h(p,c,t) \leq 0\,, \qquad (21)$$

which in the above case is simply

$$A\Omega^2 \leq \sqrt{f_{max}^2 - g^2}\,. \qquad (22)$$

The second inequality is $f_{min} \leq g$ and must be satisfied in order for a quadrocopter to land. In brief, all parameter pairs (A,Ω) satisfying the inequality (22) represent side-to-side motions that stay within the collective thrust limits (13).

However, to guarantee feasibility of the trajectory, the required motor forces must satisfy (12). In order to evaluate the motor constraints $h_i(p,c,t)$, $i \in \mathcal{I}$, we solve the dynamic equations. Note that in the following calculations, the subscript $(\cdot)_d$ is dropped to simplify notation.

For the side-to-side motion, the roll angle is zero, $\gamma(t) = 0$, for all $t \in [0,T]$. In order to fully determine the trajectory

(cf. comments in Sec. IV-B), we set the rotational rate $w_z(t)$ to zero, resulting in $\dot{\alpha}(t) = 0$, see (9). The initial yaw angle is set to zero and, thus, $\alpha(t) = 0$ for all $t \in [0, T]$. With this, the translational dynamics (7) reduce to

$$\ddot{x} = f \sin \beta \tag{23}$$
$$\ddot{z} = f \cos \beta - g. \tag{24}$$

Recalling the above results, the nominal rotational inputs (9) are $\omega = [0, \dot{\beta}, 0]$. The rotational rate $\omega_y(t)$ and the fourth input, the collective thrust f, are obtained from (23), (24) and (19), where the latter implies $\ddot{z} = 0$. From (24),

$$f = \frac{g}{\cos \beta}, \tag{25}$$

and with (23) and the second derivative of $x_d(t)$,

$$\ddot{x} = g \tan \beta \quad \Leftrightarrow \quad \beta(t) = \tan^{-1}\left(-\frac{A\Omega^2}{g} \cos(\Omega t)\right). \tag{26}$$

Equations (25) and (26) yield the inputs $\omega_y(t) = \ddot{\beta}$ and $f(t)$. Once the nominal inputs are determined, the nominal motor forces are a direct consequence of (8) and (11),

$$\begin{bmatrix} 0 & 1 & 0 & -1 \\ 1 & -1 & 1 & -1 \\ -1 & 0 & 1 & 0 \\ 1 & 1 & 1 & 1 \end{bmatrix} \begin{bmatrix} f_1 \\ f_2 \\ f_3 \\ f_4 \end{bmatrix} = \frac{1}{ml} \begin{bmatrix} 0 \\ 0 \\ I_y\ddot{\beta} \\ fl \end{bmatrix}, \tag{27}$$

where the right vector is obtained from the previous analysis and the matrix is invertible. Solving this linear system of equations results in

$$f_1 = \frac{1}{2}\left(\frac{f}{2} + \frac{I_y}{ml}\ddot{\beta}\right), \quad f_3 = \frac{1}{2}\left(\frac{f}{2} - \frac{I_y}{ml}\ddot{\beta}\right), \tag{28}$$

$$f_2 = f_4 = f/4. \tag{29}$$

The collective thrust constraint (22) guarantees the feasibility of f_2 and f_4, while the motor constraints (12) of f_1 and f_3 narrow down the set of feasible pairs (A, Ω) compared to the collective thrust inequality (22).

For the vehicle parameters in Tab. I, Fig. 4 illustrates the feasible set of side-to-side trajectories (A, Ω) for both cases. The dark gray region contains parameter sets that are infeasible due to the collective thrust limit, cf. (22). The light gray area represents the additional infeasible parameter sets obtained by taking into account the limits on the motors. Matlab files for creating the plots are available at www.idsc.ethz.ch/Downloads/QuadDance.

B. Circular Motion

As a second periodic motion primitive, we require a quadcopter to fly a circle in the horizontal plane at a constant rotational rate Ω with radius A,

$$s_d(t) = \begin{bmatrix} x_d(t) \\ y_d(t) \\ z_d(t) \end{bmatrix} = \begin{bmatrix} A\cos(\Omega t) \\ A\sin(\Omega t) \\ 0 \end{bmatrix}. \tag{30}$$
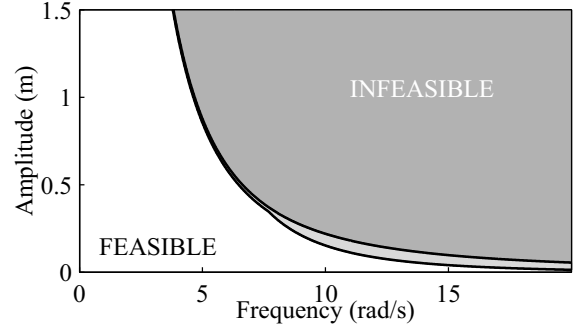

Fig. 4. Feasible parameter sets for the side-to-side motion primitive. The dark gray region denotes parameter sets that are infeasible due to collective thrust limits; light gray denotes sets that are infeasible due to additional single motor constraints.

The circle is represented by the general motion primitive description (2) with $N = 1$, $a_0 = (0,0,0)$, $a_1 = (A,0,0)$ and $b_1 = (0,A,0)$. We study the feasibility of the circle primitive depending on the parameters (A, Ω) and follow the same procedure as for the side-to-side motion in Sec. V-A.

First, the collective thrust constraint (18) is evaluated. For the circle, the nominal collective thrust is constant, cf. (17),

$$f_d = \sqrt{A^2\Omega^4 + g^2}, \tag{31}$$

resulting in the inequalities

$$A\Omega^2 \le \sqrt{f_{max}^2 - g^2}. \tag{32}$$

and $f_{min}^2 - g^2 \le A^2\Omega^4$. The latter is true for $f_{min} < g$, see Sec. V-A. Note that the same inequality, cf. (22), describes the collective thrust limit of the side-to-side primitive.

Second, we study the feasibility with respect to the motor force limits (12). For deriving the nominal rotational inputs, we transform the equations of motion into different coordinate systems, such that the flight dynamics can be described in a time-invariant manner. The subscript $(\cdot)_d$ is omitted in order to simplify notation. To describe the vehicle position, we introduce the following coordinate system $\mathbf{C}$ with (u, v, w) describing the quadrotor position in $\mathbf{C}$:

$$\begin{bmatrix} x \\ y \\ z \end{bmatrix} := R_z(\Omega t) \begin{bmatrix} u \\ v \\ w \end{bmatrix} = \begin{bmatrix} \cos\Omega t & -\sin\Omega t & 0 \\ \sin\Omega t & \cos\Omega t & 0 \\ 0 & 0 & 1 \end{bmatrix} \begin{bmatrix} u \\ v \\ w \end{bmatrix}. \tag{33}$$

The attitude of the vehicle is represented by a second set of Euler angles (η, μ, ν), describing the 'virtual vehicle attitude' $\mathbf{W}$:

$$_W^O R(\eta, \mu, \nu) = R_z(\eta) R_y(\mu) R_x(\nu), \tag{34}$$

where

$$_V^O R(\alpha, \beta, \gamma) \begin{bmatrix} 0 \\ 0 \\ 1 \end{bmatrix} = _W^O R(\eta, \mu, \nu) \begin{bmatrix} 0 \\ 0 \\ 1 \end{bmatrix}. \tag{35}$$

As every column of a rotation matrix has a unit norm, this equation defines only two of the angles (η, μ, ν). With (33), the derivatives of (33) and (35), the quadrotor's equations of
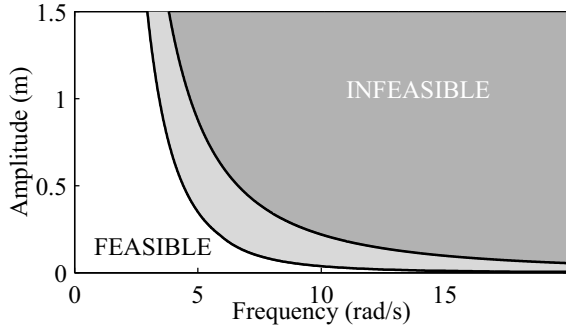
Fig. 5. Feasible parameter sets for the circular motion primitive. The dark gray region denotes parameter sets that are infeasible due to collective thrust limits; light gray denotes sets that are infeasible due to additional single motor constraints.
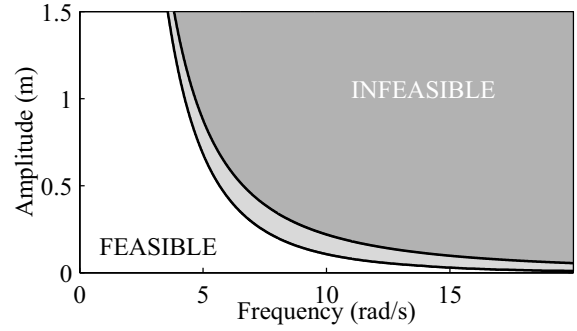

Fig. 6. Feasible parameter sets for the circular motion primitive when yaw control needs no additional control effort ($k = \infty$). The dark gray region denotes parameter sets that are infeasible due to collective thrust limits; light gray denotes sets that are infeasible due to single motor constraints.

motion (7) simplify to

$$
\begin{bmatrix} \ddot{u} \\ \ddot{v} \\ \ddot{w} \end{bmatrix} = \begin{bmatrix} f \sin\mu\cos\nu + \Omega^2 u + 2\Omega\dot{v} \\ -f\sin\nu - 2\Omega\dot{u} + \Omega^2 v \\ f\cos\mu\cos\nu - \mathrm{g} \end{bmatrix}, \qquad (36)
$$

when setting the free parameter η to $\eta = \Omega t$. The circular trajectory is described by $u = A$ and $v = 0$. Again, we have an additional design parameter to choose, see Sec. IV-C. For the circle, the vehicle rotation around its vertical axis is set to zero, i.e. $\dot{w} = 0$. Using these values and the nominal thrust (31), the Euler angles μ and ν can be calculated from (36):

$$
\mu = \arctan\left(-\frac{A\Omega^2}{\mathrm{g}}\right), \quad \nu = 0. \qquad (37)
$$

Knowing the values for (η, μ, ν), we solve for (α, β, γ) using (35). We choose $\alpha = 0$, simplifying (35) to

$$
\begin{bmatrix} \sin\beta\cos\gamma \\ -\sin\gamma \\ \cos\beta\cos\gamma \end{bmatrix} = \begin{bmatrix} \cos\Omega t\sin\mu\cos\nu + \sin\Omega t\sin\nu \\ \sin\Omega t\sin\mu\cos\nu - \cos\Omega t\sin\nu \\ \cos\mu\cos\nu \end{bmatrix}, \quad (38)
$$

which can be solved for β and γ. To calculate the rotational rate inputs in (9), we take the first derivative of (38). It can be shown that

$$
\dot{\beta} = \frac{A\Omega^3\cos^{-1}\gamma\,(\tan\beta\tan\gamma\cos(\Omega t) + \cos^{-1}\beta\,\sin(\Omega t))}{\sqrt{\mathrm{g}^2 + A^2\Omega^4}}
$$
$$ (39) $$

$$
\dot{\gamma} = \frac{A\Omega^3\cos^{-1}\gamma\cos(\Omega t)}{\sqrt{\mathrm{g}^2 + A^2\Omega^4}}. \qquad (40)
$$

Combining this result with the results from (9) and (11), one can solve for the nominal control inputs $(\omega_x, \omega_y, \omega_z)$, similar to the side-to-side motion in the previous section, Sec. V-A. The equations for the motor forces are not explicitly stated here, however Matlab files showing the relevant equations and creating the corresponding plots, see Fig. 5 and 6, are available at www.idsc.ethz.ch/Downloads/QuadDance.

Fig. 5 illustrates the feasible set of circle trajectories (A, Ω) for the vehicle parameters in Tab. I. The collective thrust limit, cf. (32), is identical to the side-to-side motion. However, the boundary that takes into account the single rotor limits is lower. One reason is that, for the circle motion,

additional rotor force is needed to keep the yaw angle at zero. Choosing the motor constant $k = \infty$, meaning that no force is required for rotational accelerations around the vertical axis of the vehicle, cf. (11), the feasible set of parameters increases, see Fig. 6. In other words, the control effort for yaw (for the given quadrocopter, see Tab. I) is large and has a noticeable effect when studying the feasibility of trajectories.

VI. PRELIMINARY EXPERIMENTAL RESULTS

We now compare the predicted feasible region of the side-to-side motion with experimental results. Experiments were conducted in the ETH Flying Machine Arena on our customized quadrocopters. The Flying Machine Arena is an indoor research space built specifically for the study of autonomous systems and aerial robotics. Details on the testbed, the vehicles, and the communication and control infrastructure are found in [15], [20].

The side-to-side motion was performed for various frequencies Ω. The amplitude was increased in small steps of 1 to 2cm starting from 0m. We monitored the commands to the motors and determined the percentage of saturated motor commands per period, hitting either the lower or upper limit of the motor, $f_{i,min}$ or $f_{i,max}$, respectively. Fig. 7 shows the experimentally obtained feasibility limits with the corresponding predicted feasibility bounds, calculated as above with the vehicle parameters in Tab. I. The vehicle parameters of our quadrocopter were determined experimentally and used before in [20], [21].

The feasibility bounds found experimentally support the predicted parameter limits. In our experiments, saturation

TABLE I

VEHICLE PARAMETER

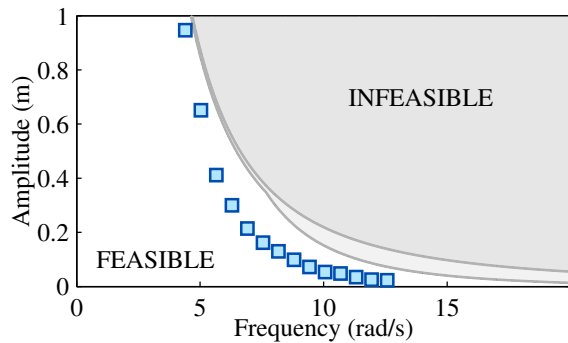|	Definition	Value
m	mass of vehicle	0.468 kg
L	vehicle arm length	0.17 m
I_x	inertia around vehicle $^V x$-axis	0.0023 kg m^2
I_y	inertia around vehicle $^V y$-axis	0.0023 kg m^2
I_z	inertia around vehicle $^V z$-axis	0.0046 kg m^2
k	motor constant	0.016 m
$f_{i,min}$	normalized min. rotor force	0.17 m/s^2
$f_{i,max}$	normalized max. rotor force	6.0 m/s^2

Fig. 7. Experimentally determined feasibility limits for the side-to-side motion. The blue boxes mark amplitudes where motor commands are saturated 1% of the time. The predicted feasibility regions are shown in gray.

occurs earlier than predicted. This can be explained by the fact that a simplified model was used when deriving the analytical bounds, see Sec. III-A. Motor dynamics, effects caused by sampling of the inputs, slew rate limits on the motor commands etc. are not considered in our analytic derivations. Moreover, additional thrust is required to stabilize the vehicle.

VII. CONCLUSION

In this paper we studied the feasibility of quadrocopter motions based on first principles models of the vehicle dynamics. We derived equations that ensure the feasibility of a desired trajectory (assumed to be twice-differentiable in time) with regard to the vehicle's collective thrust limits and the motor thrust limits. In particular, we considered motion primitives that are adjustable in their parameters. Such parameterized motion primitives will form the basis for a choreographed flight performance with quadrocopters. By adjusting the motion parameters, these primitives can capture fast/slow, smooth/sharp, and big/small motions. The goal of the feasibility analysis was to identify feasible parameter sets for these parameterized motion primitives a priori to flight experiments.

The first feasibility test used the collective thrust limit to effectively exclude most infeasible parameter combinations at little computational cost. A second feasibility test considered the thrust limits of each motor to obtain a more realistic approximation of the feasible set of trajectories. For determining the feasibility with respect to the single motors, the quadrocopter's dynamic equations must be solved for the corresponding nominal inputs. This was done for two simple examples, and the feasible parameter sets obtained from the first and second approach were compared. Our experiments validated the predicted feasibility bounds.

Ultimately, a library of these adjustable motion elements – together with their associated sets of feasible parameters – will serve as a basis for building a multifaceted choreography that is able to express different shapes, with different rhythms, in different spatial dimensions. First steps towards performing these choreographies in synchrony with music are shown in [15], [22] and accompanying videos.

REFERENCES

[1] B. Williams, M. Toussaint, and A. Storkey, "Extracting motion primitives from natural handwriting data," in *Proceedings of the International Conference on Artificial Neural Networks (ICANN)*, 2006, pp. 634–643.

[2] L. Reng, T. B. Moeslund, and E. Granum, *Finding Motion Primitives in Human Body Gestures*. Springer, 2006, pp. 133–144.

[3] S. M. LaValle, *Planning Algorithms*. Cambridge University Press, 2006.

[4] E. Frazzoli, M. A. Dahleh, and E. Feron, "Maneuver-based motion planning for nonlinear systems with symmetries," *IEEE Transactions on Robotics*, vol. 21, no. 6, pp. 1077–1091, 2005.

[5] E. Frazzoli, "Maneuver-based motion planning and coordination for multiple UAVs," in *Proceedings of the Digital Avionics Systems Conference*, vol. 2, 2002, pp. 8D3–1 – 8D3–12.

[6] D. Kulic, D. Lee, C. Ott, and Y. Nakamura, "Incremental learning of full body motion primitives for humanoid robots," in *Proceedings of the IEEE-RAS International Conference on Humanoid Robots*, 2008, pp. 326–332.

[7] S. Calinon, F. Guenter, and A. Billard, "On learning, representing, and generalizing a task in a humanoid robot." *IEEE Transactions on Systems, Man, and Cybernetics, Part B: Cybernetics*, vol. 37, no. 2, pp. 286–98, 2007.

[8] B. Hemes, D. Fehr, and N. Papanikolopoulos, "Motion primitives for a tumbling robot," *Proceedings of the IEEE/RSJ International Conference on Intelligent Robots and Systems (IROS)*, pp. 1471–1476, 2008.

[9] R. Cutler and L. Davis, "Robust real-time periodic motion detection, analysis, and applications," *IEEE Transactions on Pattern Analysis and Machine Intelligence*, vol. 22, no. 8, pp. 781–796, 2000.

[10] L. Kovar and M. Gleicher, "Automated extraction and parameterization of motions in large data sets," in *Proceedings of the International Conference on Computer Graphics and Interactive Techniques (SIGRAPH)*, 2004, pp. 559–568.

[11] R. Groten, J. Hoelldampf, M. Di Luca, M. Ernst, and M. Buss, "Motion Primitives of Dancing," *Journal of Neuroscience*, pp. 838–843, 2008.

[12] T. Shiratori, A. Nakazawa, and K. Ikeuchi, "Detecting dance motion structure through music analysis," in *Proceedings of the IEEE International Conference on Automatic Face and Gesture Recognition*, 2004, pp. 857–862.

[13] S. Nakaoka, A. Nakazawa, K. Yokoi, and K. Ikeuchi, "Leg motion primitives for a dancing humanoid robot," in *Proceedings of the IEEE International Conference on Robotics and Automation (ICRA)*, 2004, pp. 610–615.

[14] T. Shiratori, A. Nakazawa, and K. Ikeuchi, "Rhythmic motion analysis using motion capture and musical information," in *Proceedings of IEEE International Conference on Multisensor Fusion and Integration for Intelligent Systems (MFI)*, 2003, pp. 89–94.

[15] A. Schöllig, F. Augugliaro, and R. D'Andrea, "A platform for dance performances with multiple quadrocopters," in *Proceedings of the IEEE/RSJ International Conference on Intelligent Robots and Systems (IROS) - Workshop on Robots and Musical Expressions*, 2010, pp. 1–8.

[16] P. Sofras, *Dance composition basics: capturing the choreographer's craft*. Human Kinetics, 2006.

[17] S. C. Minton, *Choreography: a basic approach using improvisation*, 3rd ed. Human Kinetics, 2007.

[18] G. P. Tolstov and R. A. Silverman, *Fourier series*. Courier Dover Publications, 1962.

[19] N. Michael, D. Mellinger, Q. Lindsey, and V. Kumar, "The GRASP multiple micro UAV testbed," *IEEE Robotics and Automation Magazine*, 2010.

[20] S. Lupashin, A. Schöllig, M. Sherback, and R. D'Andrea, "A simple learning strategy for high-speed quadrocopter multi-flips," in *Proceedings of the IEEE International Conference on Robotics and Automation (ICRA)*, 2010, pp. 1642–1648.

[21] M. Hehn and R. D'Andrea, "A flying inverted pendulum," in *Proceedings of the IEEE International Conference on Robotics and Automation (ICRA)*, 2011, to appear.

[22] A. Schöllig, F. Augugliaro, S. Lupashin, and R. D'Andrea, "Synchronizing the motion of a quadrocopter to music," in *Proceedings of the IEEE International Conference on Robotics and Automation (ICRA)*, 2010, pp. 3355–3360.